Article to Journal of Materials Chemistry A

Supporting Information

Promoting Nitrate Electroreduction to Ammonia over A-site Deficient Cobalt-based Perovskite Oxides

Fulong Liu[1,#], Zhenbao Zhang[2,#], Lei Shi[3], Yu Zhang[4], Xiaoyu Qiu[5], Yuming Dong[1,*], Heqing Jiang[4], Yongfa Zhu[6,*], Jiawei Zhu[1,4,*]

[1]Key Laboratory of Synthetic and Biological Colloids, Ministry of Education, School of Chemical and Material Engineering, Jiangnan University, Wuxi 214122, China

[2]School of Chemistry and Chemical Engineering, Linyi University, Linyi 276005, China

[3]College of Materials Science and Engineering, Nanjing Forestry University, Nanjing 210037, China

[4]Qingdao Institute of Bioenergy and Bioprocess Technology, Chinese Academy of Sciences, Qingdao 266101, China

[5]School of Chemistry and Materials Science, Nanjing Normal University, Nanjing 210023, China

[6]Department of Chemistry, Tsinghua University, Beijing 100084, China

[#]These authors contributed equally to this work.

*Email: dongym@jiangnan.edu.cn, zhuyf@mail.tsinghua.edu.cn, jwzhu@qibebt.ac.cn

1 Experimental details

Chemicals and Materials. Barium nitrate ($Ba(NO_3)_2$, 99.5%), strontium nitrate ($Sr(NO_3)_2$, 99.5%), ammonium hydroxide ($NH_3 \cdot H_2O$, 25-28%), ethanol (C_2H_6O, 99.7%), isopropanol (C_3H_8O, 99.7%), potassium nitrate (KNO_3, 99.0%), potassium sulfate (K_2SO_4, 99.0%), solution of sodium hypochlorite (NaClO, available chlorine ≥ 5.2%), ammonia chloride (NH_4Cl, 99.5%), trisodium citrate dihydrate ($C_6H_5Na_3O_7$, 99.0%), salicylic acid ($C_7H_6O_3$, 99.5%), sodium thiosulfate ($Na_2S_2O_3$, AR), soluble starch from potato ($(C_6H_{10}O_5)_n$, AR), potassium iodide (KI, 99.0%), hydrochloric acid (HCl, 36-38%), sodium hydrate (NaOH, AR), and sulphuric acid (H_2SO_4, 70%) were purchased from Sinopharm Chemical Reagent. Cobalt nitrate hexahydrate ($Co(NO_3)_2 \cdot 6H_2O$, 99.99%), ferric nitrate nonahydrate ($Fe(NO_3)_3 \cdot 9H_2O$, AR), and potassium nitrate-15N ($K^{15}NO_3$, 99 atom%) were purchased from Shanghai Macklin Biochemical. Ethylenediaminetetraacetic acid (EDTA, 99.0%), and citric acid (CA, 99.5%) were purchased from Shanghai Greagent. Sodium nitroferricyanide dihydrate ($C_5FeN_6Na_2O \cdot 2H_2O$, 99.0%), and dimethyl sulfoxide (DMSO-d6, 99.9%) were purchased from Shanghai Aladdin Biochemical Technology. Maleic acid ($C_4H_4O_4$, 99.0%) was purchased from Amethyst. Nafion solution (5 wt%) was purchased from Alfa Aesar. Nafion 117 Proton exchange membrane was purchased from Dupont. Carbon black (ECP600JD) was purchased from Japan Lion. Deionized water (18.2 $M\Omega \cdot cm^{-1}$) at room temperature was used to prepare all the aqueous solutions. All chemical regents were used as received without further purification.

Preparation of catalysts. The A-site cation defective $(Ba_{0.5}Sr_{0.5})_{1-x}Co_{0.8}Fe_{0.2}O_{3-\delta}$ (x=0, 0.05, 0.10, 0.15, and 0.20, denoted as $(BS)_{1-x}CF$), were prepared by a typical sol-gel method. Firstly, stoichiometric mass of $Ba(NO_3)_2$, $Sr(NO_3)_2$, $Co(NO_3)_2 \cdot 6H_2O$, and $Fe(NO_3)_3 \cdot 9H_2O$ were dissolved in deionized water to obtain the precursor solution. Then a certain amount of EDTA-ammonium hydroxide mixture and CA were added sequentially to the precursor solution as complexing agents, and the molar ratio of total metal ions, EDTA, CA, and ammonium hydroxide was 1:1:2:10. To ensure the complexation was complete, an appropriate amount of ammonium

hydroxide was added to the mixed solution and the pH of the solution was adjusted to 7. The precursor solution was continuously magnetic stirred and heated at 90 °C for 8 h to form a transparent precursor gel. Then the precursor gel was heated at 200 °C for 5 h to obtain the solid precursor. Finally, the solid precursors were calcined in air at 950 °C for 5 h to yield pure phase perovskite-type samples. In order to make the samples more easily dispersed, the catalyst particles were mixed with ethanol and ball milled at 675 rpm·min^{-1} for 5 h. The ball-milled sample was removed and dried to get the catalyst powder with uniform particle size. Therefore, BSCF, $(BS)_{0.95}CF$, $(BS)_{0.90}CF$, $(BS)_{0.85}CF$ and $(BS)_{0.80}CF$ were successfully synthesized, respectively.

Preparation of electrode. Typically, 100 μL of Nafion solution (5 wt%) and 8 mg of mixed samples (catalyst: carbon = 1:1) were dispersed in 1900 μL of isopropanol by sonication for 2 h to form a homogeneous ink. Then, 10 μL of the above mixture was pipetted onto an L-shaped glassy carbon electrode (5 mm diameter) and dried under the atmosphere of infrared light for 30 min.

Characterization. The crystal structure of as-prepared samples were examined by room temperature X-ray diffraction (XRD, Bruker AXS, Germany D8 3 kW) and filtered Cu Kα radiation (λ = 1.5406 Å). The X-ray diffraction patterns were collected by step scanning in the 2-theta range of 20-80°with the intervals of 0.02°. *Rietveld* refinement analysis of the XRD patterns was carried out in order to obtain more detailed structural information. The specific surface area of the samples was characterized by a nitrogen adsorption test (Best Instrument Technology (Beijing), BSD-PS2) using the Brunauer-Emmett-Teller (BET) method. Scanning electron microscopy (SEM) images were conducted to observe the morphologies of as-prepared samples using a Hitachi S4800 microscope. Transmission electron microscopy (TEM) images were recorded on a JEM 2100plus microscope operating at 200 KV. The energy-dispersed X-ray (EDX) mapping images were performed on a JEOL ARM 300F with dual EDS detectors. X-ray photoelectron spectroscopy (XPS) measurements were carried out on each sample using an Axis supra spectrometer (Kratos Analytical) with an Al Kα microfused monochromatic light source. The binding energies were calibrated to an adventitious C 1s peak at 284.8 eV. The

room-temperature oxygen vacancy concentration of as-synthesized samples was determined by iodometric titration. For a typical procedure, 0.1 g of sample powder was dissolved in HCl aqueous solution under nitrogen protection to prevent the oxidation of I^- ions (from KI) by air. A few drops of starch solution were added as a titration indicator. Then, the $Na_2S_2O_3$ solution was slowly dripped into the above mixture until the end point of titration. The oxygen vacancy concentration at room temperature was calculated based on the amount of sodium thiosulfate solution.

Electrochemical measurements. Electrochemical measurements were performed in an H-type electrolytic cell separated by Nafion 117 Proton membrane, and the electrochemical data were recorded by a CS 2350M electrochemical workstation (Wuhan Corrtest). For a typical three-electrode system, Ag/AgCl (3 M KCl) electrode and platinum plate (1×1 cm^2) were used as the reference and counter electrode, respectively, and catalyst ink was applied dropwise to the glassy carbon electrode as the working electrode. A mixed electrolyte of 0.5 M KNO_3/0.1 M K_2SO_4 (50 mL) was equally distributed to the cathode and anode chambers. All potentials were recorded on the reversible hydrogen electrode ($E_{RHE} = E_{Ag/AgCl} + 0.222 + 0.0591\ V \times pH$), and then iR compensation (90%) was performed for all potentials. Prior to the nitrate electroreduction test, the electrolyte was purged with high purity Ar for 30 min. The cyclic voltammetry (CV) curves were conducted until the polarization curve reached steady state at a scan rate of 50 $mV \cdot s^{-1}$, and then the linear sweep voltammetry (LSV) curves were performed at a scan rate of 5 $mV \cdot s^{-1}$. Next, constant potential polarization tests were performed at different potentials for 0.5 h, and the produced NH_3 was analyzed by ultraviolet-visible (UV-vis) spectrophotometer and/or ^1H nuclear magnetic resonance (NMR, 400 MHz) spectroscopy. The electrochemical active surface area (ECSA) of the catalysts was evaluated using electrochemical double-layer capacitance values (C_{dl}). CV curves were performed over the non-faradaic region at scan rates of 5, 10, 20, 40, 70, and 100 $mV \cdot s^{-1}$, respectively, and the C_{dl} values were obtained from the linear relationship between the current density difference at a given potential and the scan rate. The electrochemical impedance spectra (EIS) were measured at -0.5 V (*vs*. RHE) from 0.1 Hz to 100 KHz.

Determination of ammonia. Concentration of produced NH_3 was quantified spectrophometrically by the indophenol blue method with modification.[1] Firstly, a certain amount of the reacted electrolyte was removed and diluted to 2 mL. Then, 2 mL of 1 M sodium hydroxide solution containing 5% salicylic acid and 5% sodium citrate, 1 mL of 0.05 M sodium hypochlorite and 0.2 mL of 1.0 wt% sodium nitroferricyanide solution were added. After incubation for 2 h at room temperature, the absorption spectra were measured by UV-vis. The formation of indophenol blue was measured by absorbance at 655 nm. The concentration-absorbance curves were plotted using a series of standard ammonium chloride solutions.

NMR determination of ammonia. The amount of produced NH_3 was also determined by ^1H NMR. 2 mL of the reacted electrolyte was firstly removed from the cathode chamber and neutralized by H_2SO_4 aqueous solution (2 mL, 1 M). After that, the neutralized electrolyte (30 μL) was mixed with maleic acid (as the internal standard. 10 μL, 3.6 mM) aqueous solution, H_2SO_4 aqueous solution (10 μL, 4 M), and DMSO-d6 (550 μL). A small amount of tetramethylsilane was added as a reference. All ^1H NMR experiments were performed by using pre-saturation experiments for water suppression. The concentration of NH_3 can be determined by comparing the integral area (I) of the vinylic singlets for maleic acid (6.25 ppm, 2H) with the typical triplet for ammonium (7.18 ppm, 4H) based on the following equation:[2]

$$C_{NH_4^+} = \frac{I_{NH_4^+} / H_{NH_4^+}}{I_S / H_S} \times C_S$$

where C_{NH4+} and C_S are the concentrations of ammonium and maleic acid, respectively; H_{NH4+} and H_S are the number of protons for ammonium and maleic acid, respectively; I_{NH4+} and I_S are the integrals of ^1H NMR peaks for ammonium and maleic acid, respectively. To further minimize experimental error, concentration-integrated area ratio curves were also plotted through a series of standard ammonium chloride solutions. To confirm that N element in NH_3 was derived from the NO_3^-, we performed isotope labeling experiments in 0.1 M $K^{15}NO_3$/0.1 M K_2SO_4 electrolyte, and the produced $^{15}NH_4^+$ was verified by ^1H NMR.

Calculations of NH_3 yield rate and Faradaic efficiency (FE). The NH_3 yield rate was calculated using the following equation:[3]

$$\text{yield rate}_{NH_3} = \frac{C_{NH_3} \times V}{t \times m_{cat}}$$

The NH_3 Faradaic efficiency (FE) was calculated according to following equation [3]:

$$FE_{NH_3} = \frac{C_{NH_3} \times V \times 8 \times F}{M_{NH_3} \times Q}$$

where C_{NH3} is the measured NH_3 concentration, V is the volume of the cathodic electrolyte, t is the reduction time, m_{cat} is the loading mass of catalysts, F is the Faraday constant (96485 $C \cdot mol^{-1}$), M_{NH3} is the molar mass of NH_3, and Q is the total charge passing the electrode.

2 Supplementary results

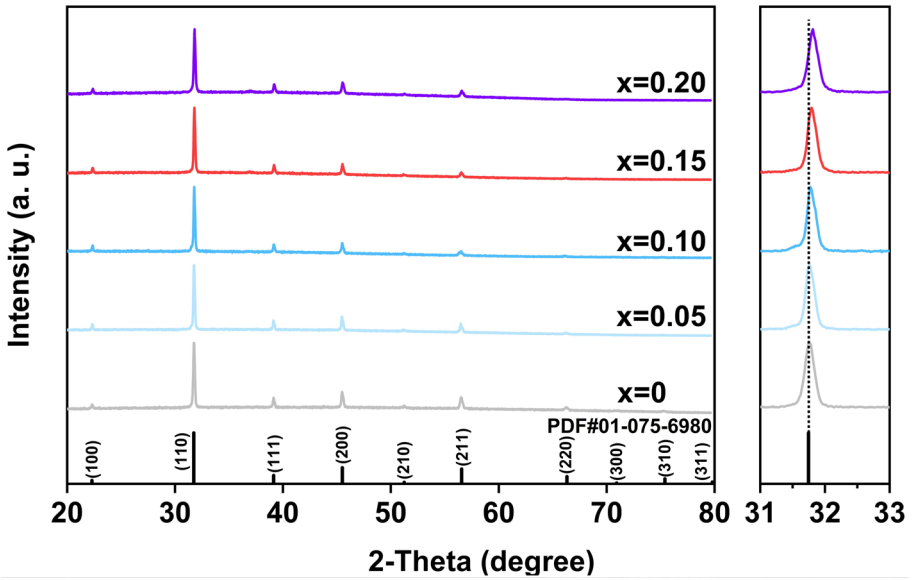

Fig. S1 XRD patterns of the $(BS)_{1-x}CF$ samples, with enlargements in the 2-theta ranges of 31-33°.

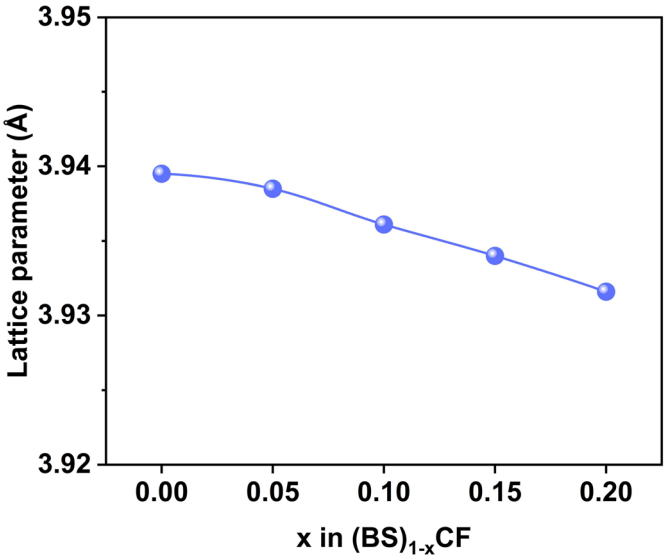

Fig. S2 Lattice parameter of the $(BS)_{1-x}CF$ samples.

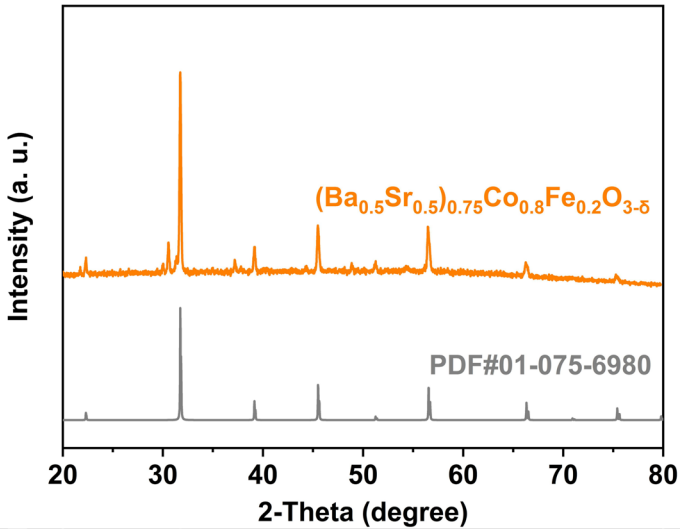

Fig. S3 XRD pattern of the $(BS)_{0.75}CF$ sample.

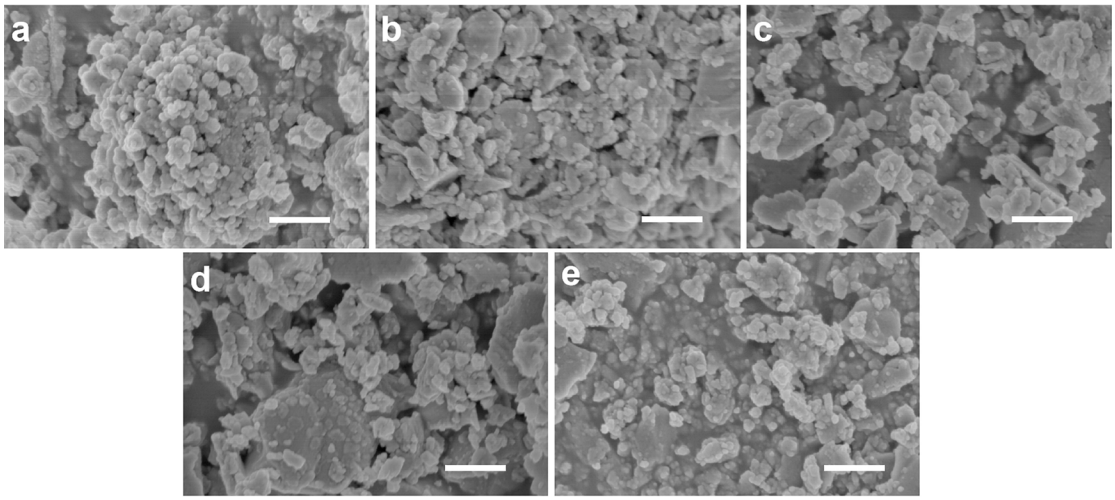

Fig. S4 SEM images of $(BS)_{1-x}CF$ samples (Scale bar: 500 nm), (**a**) BSCF, (**b**) $(BS)_{0.95}CF$, (**c**) $(BS)_{0.90}CF$, (**d**) $(BS)_{0.85}CF$, and (**e**) $(BS)_{0.80}CF$.

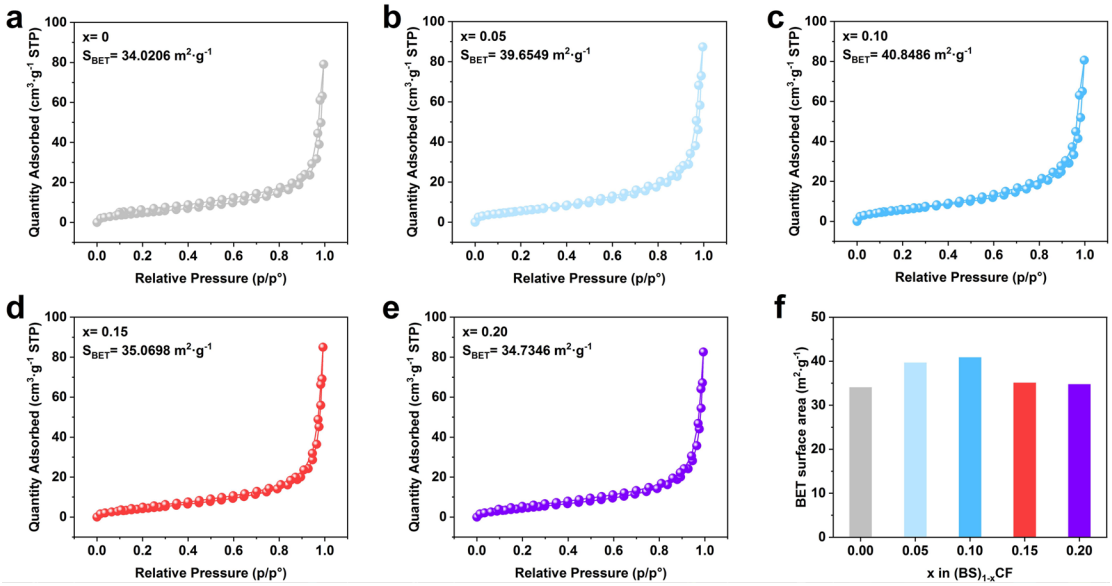

Fig. S5 N_2 adsorption-desorption isotherms of (**a**) BSCF, (**b**) $(BS)_{0.95}CF$, (**c**) $(BS)_{0.90}CF$, (**d**) $(BS)_{0.85}CF$, and (**e**) $(BS)_{0.80}CF$. (**f**) BET specific surface areas of $(BS)_{1-x}CF$ samples.

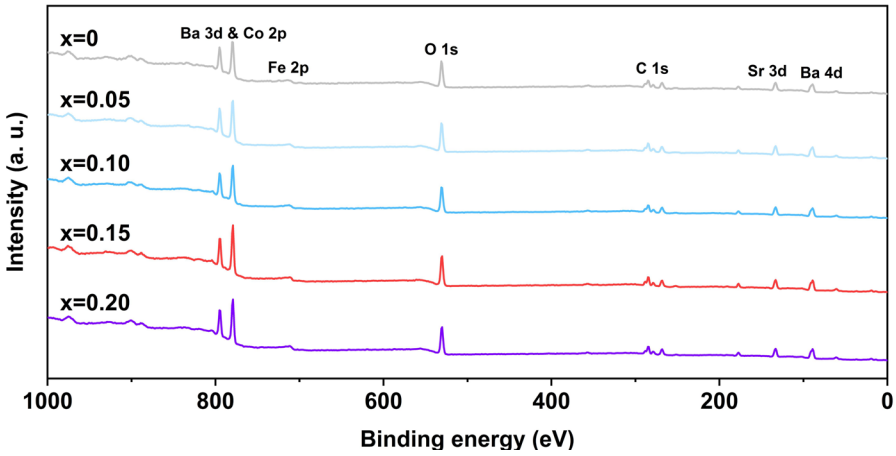

Fig. S6 Wide-scan survey XPS spectra of $(BS)_{1-x}CF$ samples.

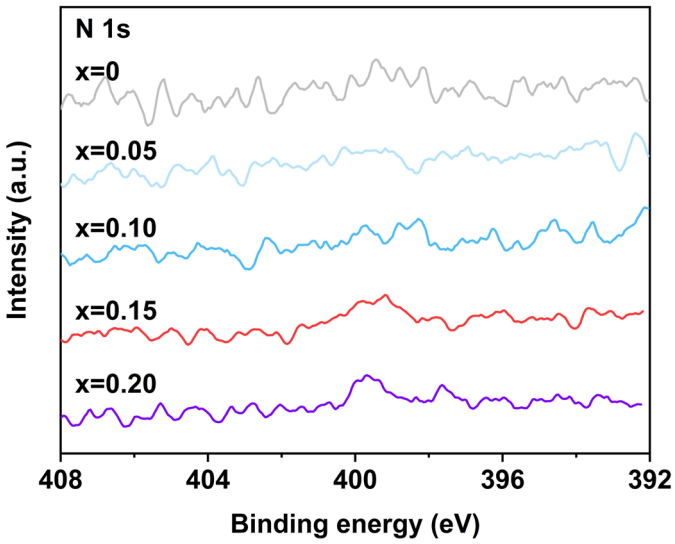

Fig. S7 N 1s XPS spectra of $(BS)_{1-x}CF$ samples.

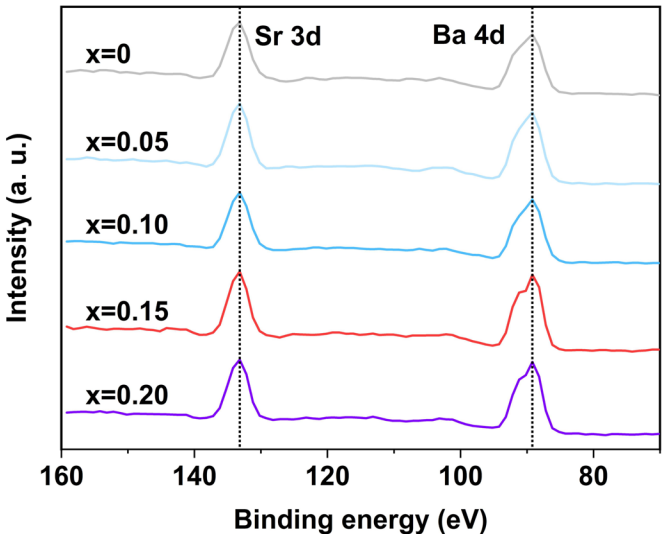

Fig. S8 Ba 4d and Sr 3d XPS spectra of the $(BS)_{1-x}CF$ samples.

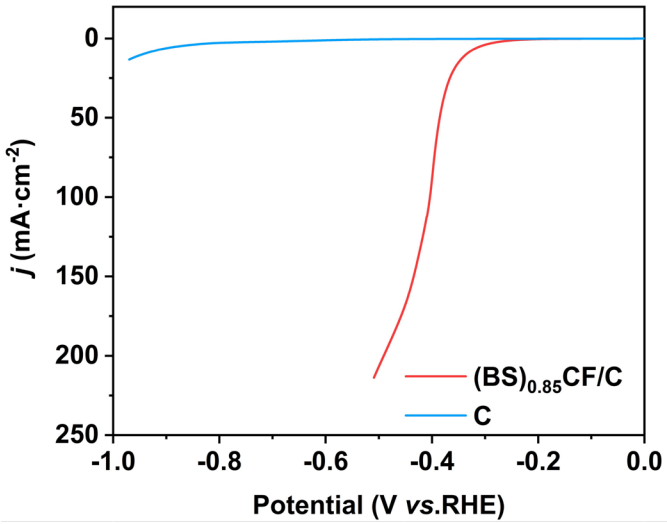

Fig. S9 LSV curves of the $(BS)_{0.85}CF/C$ and C (Carbon) in 0.5 M KNO_3/0.1 M K_2SO_4 mixed electrolyte.

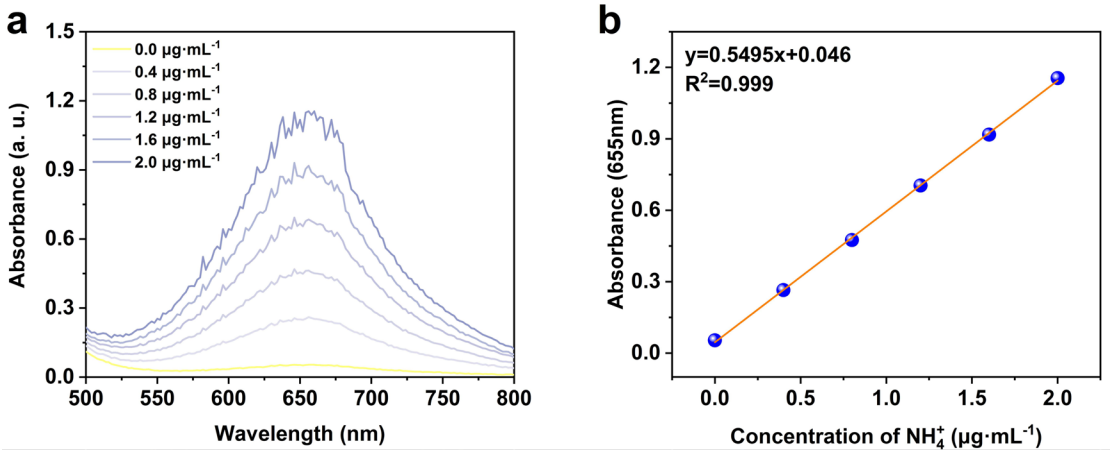

Fig. S10 UV-vis calibration curves for the determination of NH_3 in ultrapure water using a series of ammonium chloride solutions of known concentration as standards. (**a**) UV-vis curves of indophenol assays with NH_4^+ after incubated for 2 h and (**b**) calibration curve used for estimation of NH_3 by NH_4^+ of different concentrations.

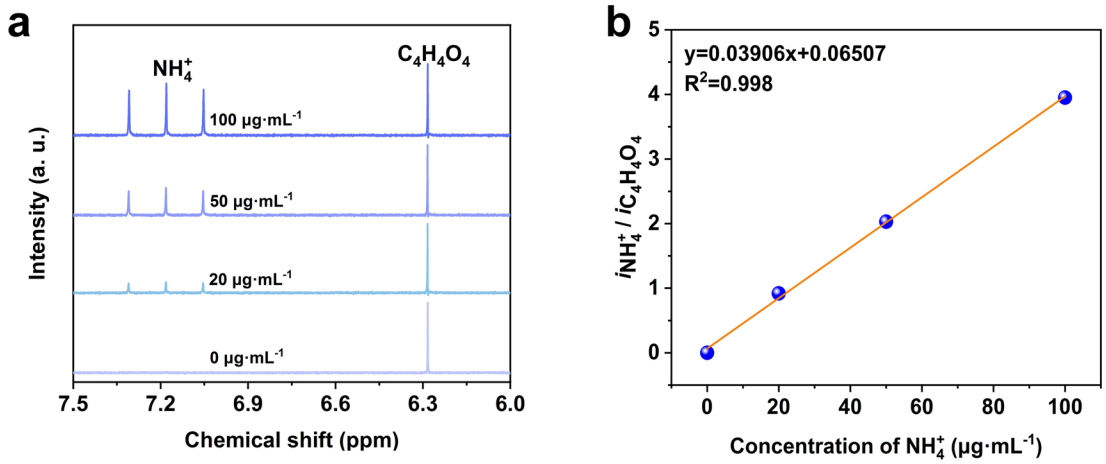

Fig. S11 ^{1}H NMR calibration curves of NH_3 in 0.5 M KNO_3/0.1 M K_2SO_4 mixed electrolyte using ammonium chloride solutions of known concentration as standards. (**a**) ^{1}H NMR spectra of NH_4^+ using maleic acid as an internal standard and (**b**) calibration curve used for estimation of NH_3 by NH_4^+ of different concentrations.

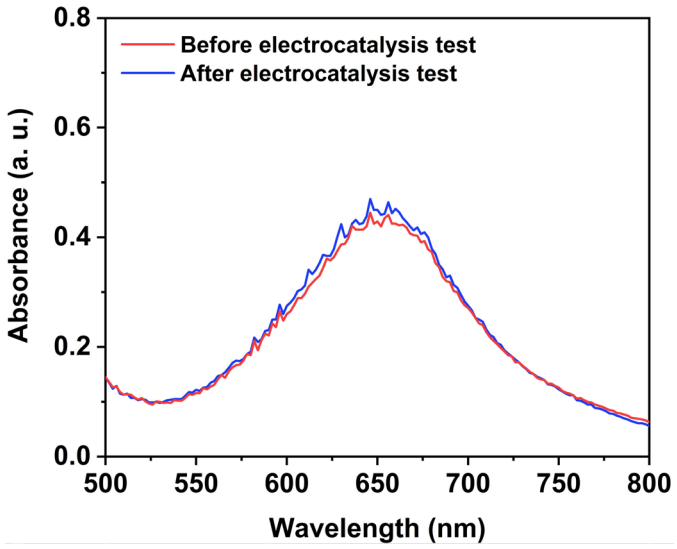

Fig. S12 UV-vis curves of electrolytes before and after electrocatalysis test for $(BS)_{0.85}CF$ in a K_2SO_4 solution without KNO_3.

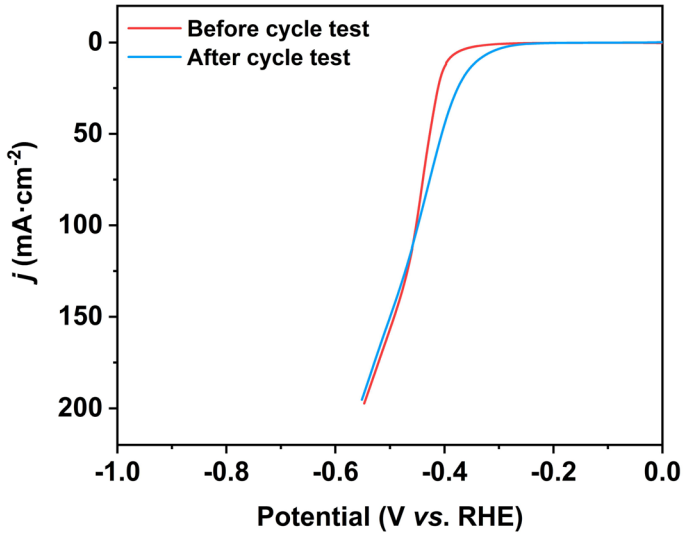

Fig. S13 LSV curves of the $(BS)_{0.85}CF$ in 0.5 M KNO_3/0.1 M K_2SO_4 mixed electrolyte before and after the cycle electrolysis test.

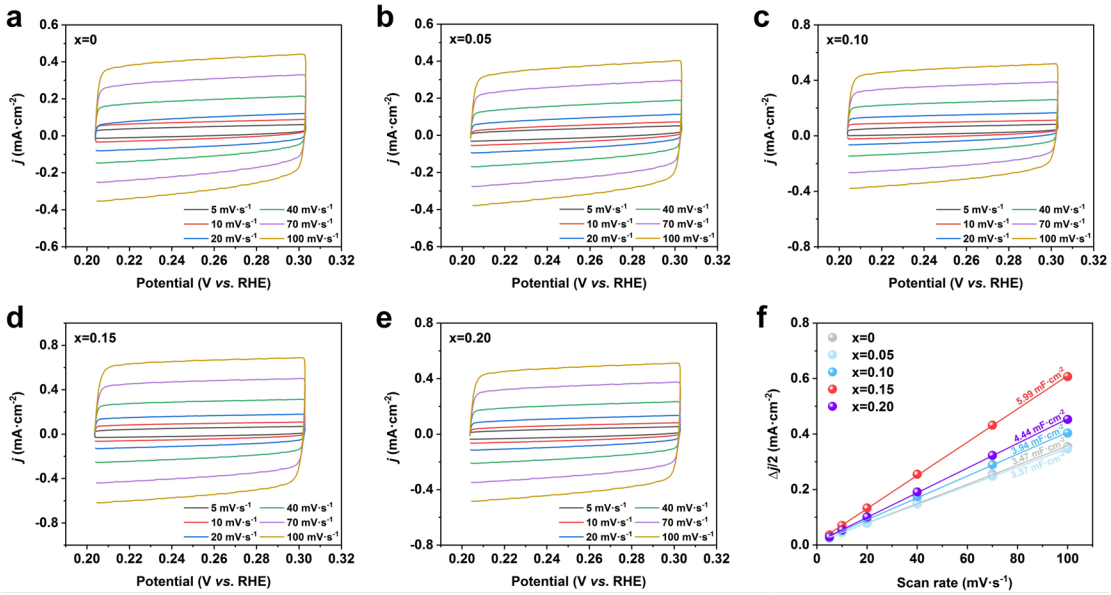

Fig. S14 CV curves with various scan rates (5, 10, 20, 40, 70, and 100 $mV \cdot s^{-1}$) of (**a**) BSCF, (**b**) $(BS)_{0.95}CF$, (**c**) $(BS)_{0.90}CF$, (**d**) $(BS)_{0.85}CF$, and (**e**) $(BS)_{0.80}CF$. (**f**) Linear fitting curves of the current density difference against scan rates of the $(BS)_{1-x}CF$ catalysts.

Table S1. Co 2p XPS peak fitting parameters and average valence state of Fe in $(BS)_{1-x}CF$ samples.

$BSCF/Co^{+3.39}$

Name	Co^{4+} $2p_{1/2}$	Co^{3+} $2p_{1/2}$	Co^{4+} $2p_{3/2}$	Co^{3+} $2p_{3/2}$
Peak position (eV)	795.6	794.2	780.4	779.0
FWHM	0.97	1.22	1.27	1.48
Peak area	8578	13295	17157	26591

$(BS)_{0.95}CF/Co^{+3.41}$

Name	Co^{4+} $2p_{1/2}$	Co^{3+} $2p_{1/2}$	Co^{4+} $2p_{3/2}$	Co^{3+} $2p_{3/2}$
Peak position (eV)	795.5	794.1	780.3	778.9
FWHM	0.89	1.16	1.08	1.39
Peak area	20368	28690	40736	57380

$(BS)_{0.90}CF/Co^{+3.41}$

Name	Co^{4+} $2p_{1/2}$	Co^{3+} $2p_{1/2}$	Co^{4+} $2p_{3/2}$	Co^{3+} $2p_{3/2}$
Peak position (eV)	795.5	794.1	780.3	778.9
FWHM	0.94	1.19	1.19	1.43
Peak area	18864	26715	37728	53430

$(BS)_{0.85}CF/Co^{+3.43}$

Name	Co^{4+} $2p_{1/2}$	Co^{3+} $2p_{1/2}$	Co^{4+} $2p_{3/2}$	Co^{3+} $2p_{3/2}$
Peak position (eV)	795.4	794.1	780.2	778.9
FWHM	0.92	0.99	1.11	1.22
Peak area	24411	31502	48823	63004

$(BS)_{0.80}CF/Co^{+3.40}$

Name	Co^{4+} $2p_{1/2}$	Co^{3+} $2p_{1/2}$	Co^{4+} $2p_{3/2}$	Co^{3+} $2p_{3/2}$
Peak position (eV)	795.4	794.1	780.2	778.9
FWHM	0.96	1.01	1.14	1.24
Peak area	20904	30759	41809	61519

Table S2. Fe 2p XPS peak fitting parameters and average valence state of Fe in $(BS)_{1-x}CF$ samples.

$BSCF/Fe^{+2.50}$

Name	Fe^{3+} $2p_{1/2}$	Fe^{2+} $2p_{1/2}$	Fe^{3+} $2p_{3/2}$	Fe^{2+} $2p_{3/2}$
Peak position (eV)	725.1	722.9	711.7	709.5
FWHM	4.00	3.37	3.27	2.6
Peak area	1048	1021	2097	2043

$(BS)_{0.95}CF/Fe^{+2.47}$

Name	Fe^{3+} $2p_{1/2}$	Fe^{2+} $2p_{1/2}$	Fe^{3+} $2p_{3/2}$	Fe^{2+} $2p_{3/2}$
Peak position (eV)	724.9	722.9	711.5	709.5
FWHM	4.00	3.10	3.16	2.60
Peak area	2270	2491	4541	4982

$(BS)_{0.90}CF/Fe^{+2.48}$

Name	Fe^{3+} $2p_{1/2}$	Fe^{2+} $2p_{1/2}$	Fe^{3+} $2p_{3/2}$	Fe^{2+} $2p_{3/2}$
Peak position (eV)	724.9	722.9	711.5	709.5
FWHM	4.00	3.16	2.98	2.69
Peak area	1998	2131	3997	4262

$(BS)_{0.85}CF/Fe^{+2.48}$

Name	Fe^{3+} $2p_{1/2}$	Fe^{2+} $2p_{1/2}$	Fe^{3+} $2p_{3/2}$	Fe^{2+} $2p_{3/2}$
Peak position (eV)	724.9	723.1	711.5	709.7
FWHM	4.00	3.32	3.29	2.83
Peak area	2697	2884	5394	5769

$(BS)_{0.80}CF/Fe^{+2.49}$

Name	Fe^{3+} $2p_{1/2}$	Fe^{2+} $2p_{1/2}$	Fe^{3+} $2p_{3/2}$	Fe^{2+} $2p_{3/2}$
Peak position (eV)	724.9	723.0	711.5	709.6
FWHM	4.00	3.52	3.37	2.89
Peak area	2762	2783	5525	5567

Table S3. The B-site average valence states and oxygen vacancy (δ) of the $(Ba_{0.5}Sr_{0.5})_{1-x}Co_{0.8}Fe_{0.2}O_{3-\delta}$ ($(BS)_{1-x}CF$) obtained by iodometric titration.

Sample		B-site average valence states	Oxygen vacancy/δ
BSCF	1	2.837	0.581
	2	2.892	0.553
	3	2.805	0.597
	Average	2.844	0.577
$(BS)_{0.95}CF$	1	2.807	0.646
	2	2.759	0.670
	3	2.860	0.619
	Average	2.808	0.645
$(BS)_{0.90}CF$	1	2.836	0.681
	2	2.784	0.707
	3	2.837	0.681
	Average	2.819	0.689
$(BS)_{0.85}CF$	1	2.843	0.728
	2	2.844	0.727
	3	2.828	0.735
	Average	2.838	0.730
$(BS)_{0.80}CF$	1	2.825	0.787
	2	2.860	0.769
	3	2.862	0.768
	Average	2.849	0.774

Table S4. O 1s XPS peak fitting parameters and the concentration of oxygen vacancies on $(BS)_{1-x}CF$ surfaces.

BSCF (O_2^{2-}/O^-)% = 38.0%

Name	Adsorbed H_2O	Adsorbed O_2/-OH	O_2^{2-}/O^-	Lattice O^{2-}
Peak position (eV)	532.8	530.9	529.4	528.6
FWHM	1.84	1.73	1.27	1.79
Peak area	4171	35424	2459	3996

$(BS)_{0.95}CF$ (O_2^{2-}/O^-)% = 39.9%

Name	Adsorbed H_2O	Adsorbed O_2/-OH	O_2^{2-}/O^-	Lattice O^{2-}
Peak position (eV)	532.8	530.9	529.4	528.7
FWHM	1.83	1.62	1.22	1.58
Peak area	9276	77404	6217	9352

$(BS)_{0.90}CF$ (O_2^{2-}/O^-)% = 49.6%

Name	Adsorbed H_2O	Adsorbed O_2/-OH	O_2^{2-}/O^-	Lattice O^{2-}
Peak position (eV)	532.9	530.9	529.4	528.6
FWHM	1.70	1.71	1.18	1.47
Peak area	7442	72593	6650	6741

$(BS)_{0.85}CF$ (O_2^{2-}/O^-)% = 53.4%

Name	Adsorbed H_2O	Adsorbed O_2/-OH	O_2^{2-}/O^-	Lattice O^{2-}
Peak position (eV)	532.8	530.9	529.4	528.7
FWHM	1.77	1.59	1.17	1.52
Peak area	8260	77815	9585	8363

$(BS)_{0.80}CF$ (O_2^{2-}/O^-)% = 55.1%

Name	Adsorbed H_2O	Adsorbed O_2/-OH	O_2^{2-}/O^-	Lattice O^{2-}
Peak position (eV)	532.9	530.9	529.4	528.7
FWHM	1.71	1.59	1.25	1.67
Peak area	7382	70280	10300	8391

Table S5. The comparison of the electrocatalytic performance of $(BS)_{0.85}CF$ with other state-of-the-art NO_3ER catalysts.

Catalyst	Electrolyte	Potential (V *vs.* RHE)	FE (%)	NH_3 Yield rate ($mg \cdot h^{-1} \cdot mg_{cat}^{-1}$)	NH_3 Yield rate ($mg \cdot h^{-1} \cdot cm^{-2}$)	Re
Fe SAC	0.1 M K_2SO_4, 0.5 M KNO_3	-0.66	~75	~20	7.82	3
FeMo−N−C	0.05 M PBS, 0.16 M KNO_3	-0.45	94.0	0.15	0.31	4
Cu Nanodisks	0.1 M KOH, 0.01 M KNO_3	-0.5	81.1	2.16		5
Bi Nanocrystals	1.0 M KOH, 0.5 M KNO_3	-0.5	90.6	46.5		6
Pd-Cu_2O	0.5 M Na_2SO_4, 50 ppm $NaNO_3$	-1.3 (V *vs*. SCE)	96.5	0.92		7
CuPd	1 M KOH, 1 M KNO_3	-0.6	92.5	106.2		8
TiO_{2-x}	0.5 M Na_2SO_4, 50 ppm $NaNO_3$	-1.6 (V *vs*. SCE)	85.0	0.76		9
Cu Nanosheets	0.1 M KOH, 10 mM KNO_3	-0.15	99.7	0.39		10
La_2CuO_4	0.5 M Na_2SO_4, 50 ppm $NaNO_3$	-0.68	75.3	1.18		11
Ni_3N	0.5 M Na_2SO_4, 0.05 M $NaNO_3$	-0.85	89.5	11.7	4.71	12
Ru Nanoclusters	1 M KOH, 1 M KNO_3	-0.2	~100	94.5	19.9	13
Pd Nanocrystalline	0.1 M Na_2SO_4, 0.1 M $NaNO_3$	-0.7	79.9	46.5	9.32	14
Cu-O_v-W	0.5 M Na_2SO_4,	-0.7	94.6	5.84		15

	0.05 M $NaNO_3$					
Zr-MOFs	0.1 M Na_2SO_4, 500 ppm NaNO3	-1.3	58.1	4.88		[16]
O-Cu–PTCDA	0.1 M PBS, 500 ppm NO_3-N	-0.4	85.9	0.43		[17]
Co_3O_4@NiO	0.5 M Na_2SO_4, 200 ppm $NaNO_3$	-0.7	54.9	0.12		[18]
$BiFeO_3$	0.1 M KOH, 0.1 M KNO_3	-0.6	96.8	90.4		[19]
1-Cu	0.5 M Na_2SO_4, 5 mM $NaNO_3$	-0.9	85.5	53.4	1.12	[20]
PdN	0.1 M Na_2SO_4, 5 mM $NaNO_3$	-0.7	96.1	3.76		[21]
$Cu/Pd/CuO_x$	0.5 M K_2SO_4, 50 mg L^{-1} KNO_3-N	-1.3 (V *vs*. SCE)	84.0	1.51		[22]
Fe SAC	0.5 M KNO_3, 0.1 M K_2SO_4	-0.68	~92	46.0		[23]
$CuFe_2O_4$	0.1 M PBS, 0.1 M NO_3^-	-1.0	91.1	9.21		[24]
Fe/CoP	1 M KOH, 50 mM KNO_3	-0.25	93.3	27.6		[25]
PPy-Cu	0.4 M K_2SO_4, 0.2 M KNO_3	-0.61	91.9	9.99		[26]
$La_xFeO_{3-\delta}$	0.1 M Na_2SO_4, 0.1 M $NaNO_3$	-0.8	78.1		1.02	[27]
$(BS)_{0.85}CF$	**0.1 M K_2SO_4, 0.5 M KNO_3**	**-0.45**	**97.9**	**143.3**	**14.6**	**This work**

References

1. D. Zhu, L. Zhang, R. E. Ruther and R. J. Hamers, *Nat Mater*, 2013, **12**, 836-841.
2. Z. Fang, Z. Jin, S. Tang, P. Li, P. Wu and G. Yu, *ACS Nano*, 2022, **16**, 1072−1081
3. E. Murphy, Y. Liu, I. Matanovic, S. Guo, P. Tieu, Y. Huang, A. Ly, S. Das, I. Zenyuk, X. Pan, E. Spoerke and P. Atanassov, *ACS Catal*, 2022, **12**, 6651-6662.
4. K. Wu, C. Sun, Z. Wang, Q. Song, X. Bai, X. Yu, Q. Li, Z. Wang, H. Zhang, J. Zhang, X. Tong, Y. Liang, A. Khosla and Z. Zhao, *ACS Mater Lett*, 2022, **4**, 650-656.
5. N. Zhang, J. Shang, X. Deng, L. Cai, R. Long, Y. Xiong and Y. Chai, *ACS Nano*, 2022, **16**, 4795-4804.
6. Y. Xu, K. Ren, T. Ren, M. Wang, Z. Wang, X. Li, L. Wang and H. Wang, *Appl Catal B Environ*, 2022, **306**, 121094.
7. Q. Gao, H. S. Pillai, Y. Huang, S. Liu, Q. Mu, X. Han, Z. Yan, H. Zhou, Q. He, H. Xin and H. Zhu, *Nat Commun*, 2022, **13**, 2338.
8. R. Jia, Y. Wang, C. Wang, Y. Ling, Y. Yu and B. Zhang, *ACS Catal*, 2020, **10**, 3533-3540.
9. X. Fu, X. Zhao, X. Hu, K. He, Y. Yu, T. Li, Q. Tu, X. Qian, Q. Yue, M. R. Wasielewski and Y. Kang, *Appl Mater Today*, 2020, **19**, 100620.
10. Z. Gong, W. Zhong, Z. He, C. Jia, D. Zhou, N. Zhang, X. Kang and Y. Chen, *Catal Today*, 2022, **402**, 259-265.
11. X. Zhang, G. Ma, L. Shui, G. Zhou and X. Wang, *Chem Eng J*, 2022, **430**, 132666.
12. J. Li, G. Zhan, J. Yang, F. Quan, C. Mao, Y. Liu, B. Wang, F. Lei, L. Li, A. W. M. Chan, L. Xu, Y. Shi, Y. Du, W. Hao, P. K. Wong, J. Wang, S. X. Dou, L. Zhang and J. C. Yu, *J Am Chem Soc*, 2020, **142**, 7036-7046.
13. Y. Han, X. Zhang, W. Cai, H. Zhao, Y. Zhang, Y. Sun, Z. Hu, S. Li, J. Lai and L. Wang, *J Colloid Interf Sci*, 2021, **600**, 620-628.
14. D. Chen, S. Zhang, X. Bu, R. Zhang, Q. Quan, Z. Lai, W. Wang, Y. Meng, D. Yin, S. Yip, C. Liu, C. Zhi and J. C. Ho, *Nano Energy*, 2022, **98**, 107338.
15. M. Jiang, J. Su, X. Song, P. Zhang, M. Zhu, L. Qin, Z. Tie, J. L. Zuo and Z. Jin, *Nano Lett*, 2022, **22**, 2529-2537.
16. Z. Y. Wu, M. Karamad, X. Yong, Q. Huang, D. A. Cullen, P. Zhu, C. Xia, Q. Xiao, M.

Shakouri, F. Y. Chen, J. Y. T. Kim, Y. Xia, K. Heck, Y. Hu, M. S. Wong, Q. Li, I. Gates, S. Siahrostami and H. Wang, *Nat Commun*, 2021, **12**, 2870.

17. G.-F. Chen, Y. Yuan, H. Jiang, S.-Y. Ren, L.-X. Ding, L. Ma, T. Wu, J. Lu and H. Wang, *Nat Energy*, 2020, **5**, 605-613.
18. Y. Wang, C. Liu, B. Zhang and Y. Yu, *Sci China Mater*, 2020, **63**, 2530-2538.
19. J. Wang, D. Wu, M. Li, X. Wei, X. Yang, M. Shao and M. Gu, *Nano Lett*, 2022, **22**, 5600-5606.
20. Y.-T. Xu, M.-Y. Xie, H. Zhong and Y. Cao, *ACS Catal*, 2022, **12**, 8698-8706.
21. L. Sun and B. Liu, *Adv Mater*, 2023, **35**, 2207.
22. T. Ren, Z. Yu, H. Yu, K. Deng, Z. Wang, X. Li, H. Wang, L. Wang and Y. Xu, *Appl Catal B Environ*, 2022, **318**, 121805.
23. W.-D. Zhang, H. Dong, L. Zhou, H. Xu, H.-R. Wang, X. Yan, Y. Jiang, J. Zhang and Z.-G. Gu, *Appl Catal B Environ*, 2022, **317**, 121750.
24. H. Zhu, S. Dong, X. Du, H. Du, J. Xia, Q. Liu, Y. Luo, H. Guo and T. Li, *Catal Sci Technol*, 2022, **12**, 4998-5002.
25. Q. L. Hong, Z. N. Zhang, X. H. Wang, S. B. Yin, F. Shi, S. N. Li and Y. Chen, *Inorg Chem*, 2022, **61**, 14397-14402.
26. Z. Li, L. Wang, Y. Cai, J.-R. Zhang and W. Zhu, *J Hazard Mater*, 2022, **440**, 129828.
27. Q. Yin, S. Hu, J. Liu and H. Zhou, *Sustain Energ Fuels*, 2022, **6**, 4716-4725.